

---

# TRIMMING THE FAT: EFFICIENT COMPRESSION OF 3D GAUSSIAN SPLATS THROUGH PRUNING

---

A PREPRINT

**Muhammad Salman Ali<sup>1,2</sup>, Maryam Qamar<sup>2</sup>, Sung-Ho Bae<sup>2</sup>, Enzo Tartaglione<sup>1</sup>**

<sup>1</sup>LTCI, Télécom Paris, Institut Polytechnique de Paris, France

<sup>2</sup>Kyung Hee University, Republic of Korea

{salmanali,maryamqamar,shbae}@khu.ac.kr,  
{enzo.tartaglione}@telecom-paris.fr

## ABSTRACT

In recent times, the utilization of 3D models has gained traction, owing to the capacity for end-to-end training initially offered by Neural Radiance Fields and more recently by 3D Gaussian Splatting (3DGS) models. The latter holds a significant advantage by inherently easing rapid convergence during training and offering extensive editability. However, despite rapid advancements, the literature still lives in its infancy regarding the scalability of these models. In this study, we take some initial steps in addressing this gap, showing an approach that enables both the memory and computational scalability of such models. Specifically, we propose “Trimming the fat”, a post-hoc gradient-informed iterative pruning technique to eliminate redundant information encoded in the model. Our experimental findings on widely acknowledged benchmarks attest to the effectiveness of our approach, revealing that up to 75% of the Gaussians can be removed while maintaining or even improving upon baseline performance. Our approach achieves around 50 $\times$  compression while preserving performance similar to the baseline model, and is able to speed-up computation up to 600 FPS.

**Keywords** 3D Gaussian Splatting · Pruning · Compression.

## 1 Introduction

In the last few years, significant advancements have been made in radiance field methodologies for reconstructing 3D scenes using images captured from various viewpoints. The emergence of Neural Radiance Fields (NeRF) techniques has notably influenced the realm of 3D scene modeling and reconstruction [1, 2]. The efficient generation of photo-realistic novel views from a given set of training images has become a focal point in computer vision research, with diverse applications [3]. NeRF’s capability to distill the essence of a 3D object from its 2D representations, while maintaining compactness, underscores its impact and popularity in the literature [4, 5].

Despite its success, the traditional NeRF [1] suffers from slow training and rendering speeds. To address this challenge, various approaches have been proposed, although they often entail compromises in rendered image quality [3]. Recent studies have turned to explicit scene representations, such as voxel-based [6] or point-based [7] structures to enhance rendering efficiency. For instance, leveraging 3D voxel grids on GPUs alongside multi-resolution hash encoding of inputs led to consistent reductions in required operations and enabled real-time performance [8]. Similarly, the most efficient radiance field solutions to date rely on continuous representations achieved through interpolating values stored in voxel [9], hash grids [8], or points [7]. While the continuous nature of these methods aids optimization, the stochastic sampling necessary for rendering can incur computational overhead and introduce noise [10].

A recent advancement in the field is the introduction of differentiable 3D Gaussian splatting (3DGS), which enables the generation of a sparse adaptive scene representation [10]. This representation can be rendered rapidly on the GPU, offering big speed improvements. 3DGS combines the best features of existing methods: leveraging a 3D Gaussian representation for scene optimization provides state-of-the-art visual quality and competitive training times while the tile-based splatting solution ensures real-time rendering at high quality for 1080p resolution across various datasets. Unlike NeRF methods, 3DGS simplifies training and rendering by projecting 3D Gaussians to the 2D image space and combines them with opacity using *rasterization*, enabling real-time rendering on a single GPU. Furthermore, the

explicit storage of scene structure in the parameter space allows for direct editing of the 3D scene. However, some challenges emerge when employing differentiable 3DGS, particularly in optimizing scenes with millions of Gaussians, which may require substantial storage and memory. While specialized pipelines demonstrate real-time performance on high-end GPUs, seamless integration into VR/AR environments or games remains a challenge, particularly when working alongside hardware rasterization of polygon models.

In this paper, we aim to compress Gaussian splatting representations while preserving their rendering speed and quality, facilitating their application across diverse domains such as IoT devices with limited storage or memory. Our primary insight is that the learned 3DGS models exhibit over-fitting to the underlying scene, allowing for the removal or pruning of many Gaussians without sacrificing performance, particularly due to markedly lower opacity values. We start the training process with a pre-trained optimized Gaussian scene, iteratively pruning it based on opacity levels and gradient values compared to the baseline optimized scene as showcased from Fig. 1. Our main contributions are the following.

- We build on top of the optimized 3DGS as a 3D prior for pruning, enabling the removal of redundant Gaussians while fine-tuning the remaining ones to accurately capture the scene features (Sec. 3.2).
- We observe that vanilla pruning is sub-optimal when compared to a gradient-informed approach and that pruning without such a prior fails. Besides, we showcase the compatibility with other compression pipelines, like [11] (Sec. 4.3).
- With our proposed method, we achieve state-of-the-art performance even after pruning 50% of the Gaussian splats, significantly enhancing the scalability of 3DGS (Sec. 4.2). Our compression pipeline achieves an enhanced balance between scene fidelity and compression, surpassing the baseline (Fig. 6).

## 2 Related Work

In this section we first provide an overview of the most recent methods for novel view synthesis (Sec. 2.1), then we discuss approaches for their compression (Sec. 2.2).

### 2.1 Novel View Synthesis

Recent advancements in novel view synthesis have seen significant progress, with early techniques using CNNs to estimate blending weights or texture-space solutions [12, 13, 14, 15], albeit facing challenges with MVS-based geometry and temporal flickering. Volumetric representations, starting with Soft3D [16] and employing deep learning with volumetric ray-marching [17, 18], provided further advancements. Neural Radiance Fields (NeRFs) [1] aimed to enhance synthesized views’ quality but faced slow processing due to a large Multi-Layer Perceptron (MLP) backbone and dense sampling. Subsequent methods like Mip-NeRF360 [19] focused on balancing quality and speed, while recent advances prioritize faster training and rendering through spatial data structures, encodings, and MLP adjustments [20, 9, 21]. Notable methods such as InstantNGP [8] leverage hash grids and occupancy grids for accelerated computation, while Plenoxels [9] rely on Spherical Harmonics for directional effects without neural networks. Despite these strides, challenges persist in NeRF methods regarding efficient coding for empty space, image quality, and rendering speed.

In contrast, 3DGS achieves superior quality and faster rendering without implicit learning. However, its increased storage compared to NeRF methods poses limitations. Our approach aims to maintain the quality and speed of 3DGS while reducing model storage by applying pruning to Gaussian parameters.

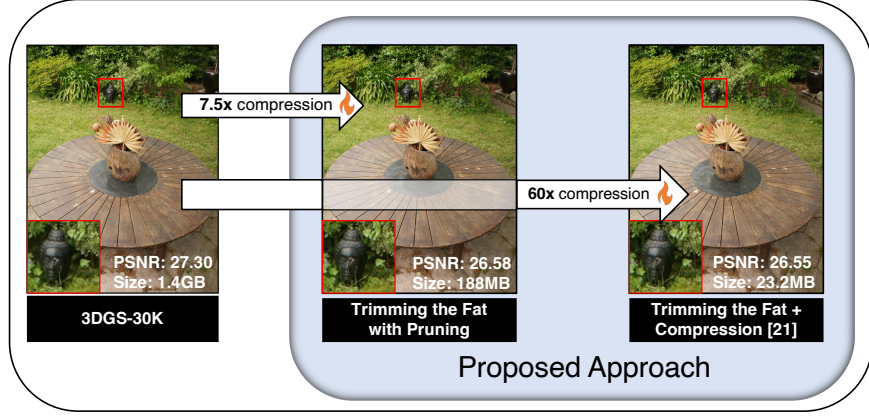


Figure 1: Vanilla 3DGS-30k VS our novel pruning approach applied with an end-to-end compression technique [11].

followed by fine-tuning to achieve superior performance-compression trade-off compared to the baseline optimized scene as showcased from Fig. 1. Our main contributions are the following.

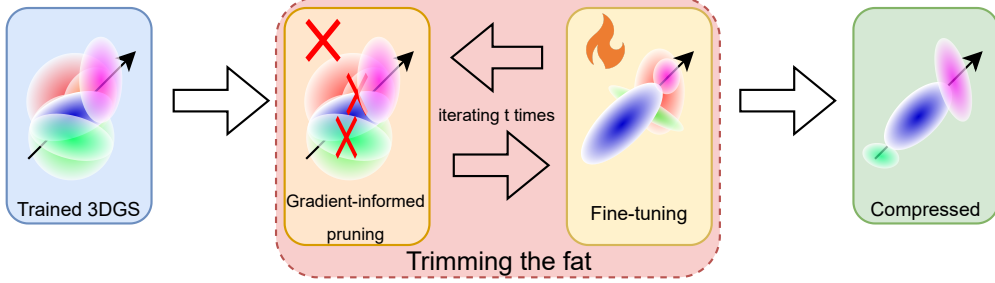


Figure 2: Overview of our pruning pipeline. From a pre-trained 3DGS-30k scene, we first iteratively prune it for a fixed number of iterations with subsequent fine-tuning. Then, we conduct further fine-tuning for 20,000 iterations to obtain our final optimized scene.

## 2.2 3DGS Compression

When compared to NeRFs, 3DGS models lack structure, which presents challenges for compression [22, 23]. Consequently, many studies in 3DGS compression introduce structural parameters by replacing vanilla 3DGS parameters to enhance compression [24, 22]. Scaffold-GS [24], for instance, utilizes anchor points to distribute local 3D Gaussians and predicts their attributes dynamically based on the viewing direction and distance within the view frustum. On the other hand, the Hash-grid Assisted Context (HAC) [22] framework jointly learns a structured compact hash grid and uses it for context modeling of anchor attributes.

Niedermayr *et al.* [11] proposed a compression framework that maintains vanilla 3DGS parameters while compressing directional colors and Gaussian parameters. This framework incorporates sensitivity-aware vector clustering and quantization-aware training and achieves compression rates of up to  $30\times$  with a marginal decline in performance compared to the baseline 3DGS. Another method, Compact3D [25], introduces a learnable mask strategy to prune the Gaussians and a compact representation of view-dependent colors by employing a grid-based neural field rather than relying on spherical harmonics. It also learns codebooks to compactly represent the geometric attributes of Gaussian by vector quantization.

Our proposed pruning method can effectively improve/replace the masking strategies for unimportant Gaussians in the existing works (see Sec. 4.2). However, for the scope of this paper and considering the broad applicability of vanilla 3DGS, we focus solely on the vanilla 3DGS variant.

## 3 Methodology

In this section, we first provide an overview of the 3DGS technique for learning and rendering 3D scenes, as introduced by Kerbl *et al.* [10] (Sec. 3.1). Then, we delve into an explanation of our pruning approach (Sec. 3.2). Our methodology, depicted in Fig. 2, introduces an effective approach to compress these models using gradient-informed pruning.

### 3.1 Differentiable Gaussian Splatting

3DGS [10] represents a scene through a set of 3D Gaussians. By leveraging differentiable Gaussian splatting, which extends EWA volume splatting [26], it facilitates the efficient projection of 3D Gaussian kernels onto the 2D image plane. Additionally, differentiable rendering optimizes the quantity and attributes of the Gaussian kernels employed to characterize the scene. Each 3D Gaussian is characterized by its position and covariance matrices within the 3D space, modeled as

$$G(x) = \exp \left[ -\frac{1}{2}(x - \mu)^T \Sigma^{-1} (x - \mu) \right], \quad (1)$$

where  $x$  denotes the position vector,  $\mu$  represents the position, and  $\Sigma$  is the 3D covariance matrix of the Gaussian distribution. Given the requirement for the covariance matrix to be positive definite, it can be parameterized using a rotation matrix  $R$  and a scaling matrix  $S$ . To facilitate independent optimization of  $R$  and  $S$ , Kerbl *et al.* [10] introduce a representation of rotation via a quaternion  $q$  and scaling through a vector  $s$ , both of which can be converted into their corresponding matrices. Additionally, each Gaussian distribution possesses its opacity ( $\alpha \in [0, 1]$ ) and a set of spherical harmonics (SH) coefficients essential for reconstructing a view-dependent color. The 2D projection of a 3D Gaussian

remains a Gaussian with covariance

$$\Sigma' = JW\Sigma W^T J^T, \quad (2)$$

where  $W$  is the view transformation matrix, and  $J$  is the Jacobian of the affine approximation of the projective transformation. This setup facilitates the evaluation of the 2D color and opacity footprint of each projected Gaussian. The color  $C$  of a pixel is subsequently determined by blending all the  $N$  2D Gaussians contributing to that pixel:

$$C = \sum_{i \in N} c_i \alpha_i + \prod_{j=1}^{i-1} (1 - \alpha_j), \quad (3)$$

where  $c_i$  and  $\alpha_i$  represent the view-dependent color and opacity of a Gaussian, respectively, which are adjusted based on the exponential decay from the center point of the projected Gaussian. The parameters such as position  $x$ , rotation  $q$ , scaling  $s$ , opacity  $\alpha$ , and spherical harmonics (SH) coefficients of each 3D Gaussian are optimized to ensure alignment between the rendered 2D Gaussians and the training images.

During the training phase, the 3D Gaussian splats are rendered efficiently in a differentiable manner to produce a 2D image. This rendering process involves  $\alpha$ -blending of anisotropic splats, sorting them, and utilizing a tile-based rasterizer. At each training iteration, the 3DGS framework renders the training viewpoints and then minimizes the loss between the ground truth and rendered images in the pixel space, where the loss is given by

$$\mathcal{L} = (1 - \lambda) \mathcal{L}_1 + \lambda \mathcal{L}_{\text{D-SSIM}}, \quad (4)$$

where  $\mathcal{L}_1$  is the  $\ell_1$  norm of the rendered output and  $\mathcal{L}_{\text{D-SSIM}}$  is its structural dissimilarity. The optimization in 3DGS begins with a point cloud generated through a conventional SfM method [27], and then proceeds iteratively, pruning Gaussians with small opacity parameters and introducing new ones when significant gradients are detected. As demonstrated in the 3DGS paper, this approach enables rapid training and facilitates real-time rendering, all while achieving comparable or superior 3D model quality compared to state-of-the-art NeRF methods.

### 3.2 Gradient Aware Pruning

3DGS typically necessitates several million Gaussians to adequately model a standard scene, each Gaussian entailing 59 parameters. This results in a storage size significantly larger than that of most NeRF methodologies, such as Mip-NeRF360 [19], K-planes [28], and InstantNGP [8]. Such requirements render 3DGS inefficient for certain applications, particularly those involving edge devices. Our primary focus is on parameter reduction. In the original training process of 3DGS, Kerbl *et al.* [10] pruned and densified Gaussians up to a specified number of iterations, with pruning based on a predetermined opacity threshold. However, if their opacity is low and so is its gradient, we can say they can be removed with little to no impact on the quality of the rendered scene. As such, we have

$$\Sigma' = \begin{cases} \Sigma_i & \text{if } [|\Sigma_i^\alpha| \geq \mathcal{Q}_{|\Sigma^\alpha|}(\gamma_{\text{iter}})] \vee [|\nabla \Sigma_i| \geq \mathcal{Q}_{|\nabla \Sigma|}(\gamma_{\text{iter}})] \\ 0 & \text{otherwise,} \end{cases} \quad (5)$$

where  $\Sigma_i^\alpha$  denotes the  $\alpha$  value of the  $i$ -th Gaussian, and  $\nabla \Sigma_i$  denotes the gradient for the  $i$ -th Gaussian,  $\mathcal{Q}_{|\Sigma^\alpha|}(\cdot)$  represents the quantile function for the opacity,  $\mathcal{Q}_{|\nabla \Sigma|}(\cdot)$  is the quantile function for the gradients of the Gaussians, and  $\gamma \in [0, 1]$  denotes the fraction of Gaussians to be removed. This pruning process, along with periodic fine-tuning, not only improves performance but evidently results in substantial compression gains.

The iterative pruning and fine-tuning approaches enable the removal of redundant Gaussians while refining the remaining ones to better capture scene details compared to the baseline. Prior research in scene rendering has demonstrated that a gradual iterative pruning strategy can yield significantly sparser models while preserving high fidelity [3]. However, the impact of such an approach on 3DGS models yet remains unclear. We speculate that by gradually pruning the model over a specified number of iterations  $t$  and aiming for a target sparsity  $\gamma_{\text{target}}$ , we can achieve improved results through a sparsification process applied to the 3DGS model: at every iteration, we apply the sparsification

$$\gamma_{\text{iter}} = 1 - (1 - \gamma_{\text{target}})^{\frac{1}{t}}. \quad (6)$$

Our approach is based on two key factors. First, during the fine-tuning stage following pruning, the covariance  $\Sigma$  is adjusted to minimize rendering loss, leading to higher values for solid surfaces and lower values for semi-transparent artifacts, which can be subsequently removed in the next iteration (which will be empirically observed in Fig. 7c). Second, the gradual iterative process helps prevent the optimization algorithm from converging to sub-optimal local minima (according to empirical evidence discussed in Sec. 4.3). Hence, it is crucial to initiate the process with an overparametrized yet well-performing model. Similar observations can be drawn from traditional deep learning literature [29, 30]. In the next section, we will present a quantitative analysis of typical benchmarks employed for 3DGS.

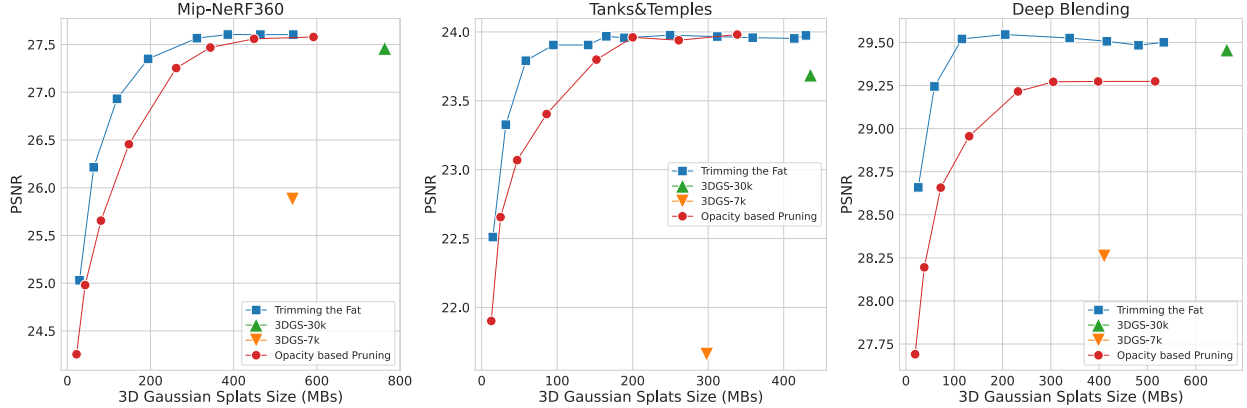


Figure 3: The graph depicts the trade-off between performance and size when utilizing Trimming the Fat (gradient-aware iterative pruning) compared to the 3DGS-30k and 3DGS-7k baselines as well as opacity-based pruning on the Mip-NeRF360, Tanks&Temple, and Deep Blending datasets.

Model	$\gamma_{\text{iter}}$	Mip-NeRF360				Tanks&Temples				Deep Blending			
		SSIM $\uparrow$	PSNR $\uparrow$	LPIPS $\downarrow$	Mem $\downarrow$	SSIM $\uparrow$	PSNR $\uparrow$	LPIPS $\downarrow$	Mem $\downarrow$	SSIM $\uparrow$	PSNR $\uparrow$	LPIPS $\downarrow$	Mem $\downarrow$
3DGS-7k $^{\dagger}$	-	0.770	25.60	0.279	523.00	0.767	21.20	0.280	270.00	0.875	27.78	0.317	386.00
3DGS-30k $^{\dagger}$	-	0.815	27.21	0.214	734.00	0.841	23.14	0.183	411.00	0.903	29.41	0.243	676.00
3DGS-7k $^{*}$	-	0.765	25.88	0.288	541.70	0.777	21.66	0.266	298.00	0.876	28.26	0.312	410.50
3DGS-30k $^{*}$	-	0.812	27.46	0.221	763.40	0.845	23.69	0.178	435.50	0.899	29.46	0.246	664.50
3DGS- Opacity Based Pruning	0.025	0.813	27.58	0.217	592.22	0.849	23.98	0.169	338.50	0.894	29.27	0.248	516.00
	0.050	0.813	27.56	0.220	449.11	0.849	23.94	0.171	261.00	0.894	29.27	0.250	398.00
	0.075	0.809	27.47	0.231	344.00	0.846	23.96	0.178	200.00	0.895	29.27	0.252	305.00
	0.100	0.799	27.25	0.250	261.78	0.839	23.80	0.192	152.00	0.894	29.22	0.259	232.00
	0.150	0.762	26.46	0.304	148.00	0.818	23.40	0.232	86.00	0.888	28.96	0.279	131.00
	0.200	0.725	25.66	0.353	80.89	0.794	23.07	0.574	47.00	0.883	28.66	0.295	72.00
	0.250	0.692	24.98	0.394	42.78	0.767	22.66	0.310	25.00	0.877	28.20	0.310	38.00
Trimming the Fat	0.300	0.659	24.26	0.430	22.14	0.731	21.90	0.354	12.65	0.869	27.69	0.328	19.00
	0.225	0.813	27.60	0.217	543.44	0.849	23.96	0.170	335.50	0.898	29.50	0.247	534.00
	0.275	0.814	27.60	0.219	464.33	0.849	23.97	0.171	280.75	0.898	29.48	0.247	481.50
	0.325	0.813	27.60	0.223	386.11	0.848	23.97	0.175	219.25	0.899	29.51	0.248	416.00
	0.375	0.810	27.57	0.231	311.78	0.844	23.94	0.187	153.00	0.899	29.53	0.250	339.00
	0.450	0.797	27.35	0.256	194.22	0.829	23.85	0.220	76.75	0.899	29.55	0.253	205.50
	0.500	0.776	26.93	0.288	119.44	0.810	23.56	0.251	45.25	0.899	29.52	0.258	116.00
	0.550	0.740	26.21	0.336	63.56	0.780	22.92	0.294	23.38	0.897	29.25	0.269	59.00
	0.600	0.690	25.03	0.394	29.22	0.761	22.51	0.319	14.75	0.887	28.66	0.293	25.50

Table 1: Performance comparison using Trimming the Fat (gradient-aware iterative pruning) with different pruning levels defined by  $\gamma_{\text{iter}}$  against 3DGS-30k, 3DGS-7k baselines, and opacity-based iterative pruning. \* Reproduced using official code.  $^{\dagger}$  Reported from [10]. Memory size is in MBs.

## 4 Experiments and Results

In this section, we present our empirical findings on commonly recognized benchmarks within the 3DGS community. We begin by detailing the implementation of our approach, followed by an outline of the benchmarked datasets and the evaluation metrics employed (Sec. 4.1). Subsequently, we discuss both qualitative and quantitative results (Sec. 4.2), providing as well an ablation study (Sec. 4.3).

### 4.1 Implementation Details

In all our experiments, we use the publicly available official code repository of 3DGS [10], adhering to the recommended hyperparameter settings used for training to maintain consistency with the original 3DGS model. We initiate the pruning process with the optimized Gaussians trained for 30,000 iterations, employing pruning with  $\gamma_{\text{iter}} \in [0.225, 0.6]$ , as described in (5). Iterative pruning with the same  $\gamma_{\text{iter}}$  value is applied after every 500 iterations until reaching 35,000 iterations (commencing from 30,000 iterations), followed by further fine-tuning for 10,000 iterations. For all our experiments, pruning and fine-tuning consistently yield significantly improved compression-performance trade-offs.



Figure 4: Qualitative comparison of the train scene at various pruning levels, defined by  $\gamma_{\text{iter}}$  using Trimming the Fat (gradient-aware iterative pruning). Our proposed method demonstrates substantially higher compression rates compared to both baselines while maintaining similar visual quality.

Additionally,  $\lambda = 0.2$  is employed consistently across all our experiments. **Datasets.** We assess the efficacy of our pruning approach across diverse scenes, encompassing environments from the Mip-Nerf360 [19] indoor and outdoor datasets, alongside two scenes sourced from the Tanks&Temples [31] and Deep Blending [13] datasets, akin to the scenes examined in the original 3DGS work [10].

**Evaluation.** To ensure a fair comparison, we adhere to the same train-test split utilized in Mip-Nerf360 [19] and 3DGS [10]. Our evaluation encompasses standard metrics like SSIM, PSNR, and LPIPS, alongside the average memory consumption across all datasets.

## 4.2 Results

### 4.2.1 Quantitative Comparison

**Trimming the Fat.** We conduct a comparative analysis between our method, the 3DGS-30k, and 3DGS-7k baselines, along with an opacity-based pruning approach that removes gradient information from (5). As illustrated in Table 1 and Fig. 3, we examine the trade-off in compression performance across benchmark datasets. Across all the datasets, Gaussian splats can be pruned by up to  $4\times$ , showcasing improved or similar performance compared to the baseline. Notably, even at significantly high pruning levels, where the average scene size is less than 25MB, our proposed pruning technique maintains comparable or even superior performance to that of the 3DGS-7k variant, achieving compression rates of up to  $24\times$  on average. This is realized without the need for any additional end-to-end compression pipeline integration, highlighting the standalone scalability of our proposed approach.

Opacity-based pruning exhibits similar performance to gradient-aware pruning at small pruning thresholds. However, the performance difference becomes more pronounced at higher compression rates, as evident from the results in Fig. 3. Incorporating gradient information leads to additional performance improvements in pruning. This enhancement arises because certain scene features (sky, glass, etc.) may have low opacity but are still crucial for overall scene rendering.



Figure 5: Qualitative comparison of the playroom scene at various pruning levels, defined by  $\gamma_{\text{iter}}$  using Trimming the Fat (gradient-aware iterative pruning). Our proposed method demonstrates substantially higher compression rates compared to both baselines while maintaining similar visual quality.

By considering gradient information, we ensure that only Gaussians containing unimportant features are pruned. Our proposal of incorporating information on the gradient shows its prominent effectiveness at higher pruning rates.

**Trimming the Fat with end-to-end compression.** Our proposed pruning methodology can act as a plug-and-play with various end-to-end compression techniques for 3DGS. When integrated with the method proposed by [11], we achieve state-of-the-art compression performance. Niedermayr’s approach begins with a pre-trained Gaussian as the foundation of its compression process. We substitute this pre-trained Gaussian with our pruned Gaussian and apply the end-to-end compression procedure. This combination results in  $50\times$  compression compared to the baseline, while maintaining comparable performance. Moreover, we achieve  $2\times$  compression with improved performance compared to Niedermayr’s original approach, as demonstrated in Table 2.

#### 4.2.2 Qualitative Comparison

We present visualizations of train scene from the Tanks&Temples dataset, playroom scene from the Deep Blending dataset, and the garden scene from the Mip-NeRF360 dataset all of which require substantial memory resources on average. In Fig 4, 5 and 6, we illustrate the visualizations of test set images at various pruning levels indicated by  $\gamma_{\text{iter}}$ . Our “trimming the fat” iterative pruning pipeline achieves noteworthy compression rates while maintaining comparable visual quality. Across all scenes depicted in the Fig. 4, 5 and 6 our method compresses the Gaussian splats by approximately  $4\times$  with visual quality similar to 3DGS-30K. Furthermore, with  $\gamma = 0.60$ , our method achieves an average compression ratio of approximately  $22\times$  while preserving visual quality comparable to 3DGS-7K.

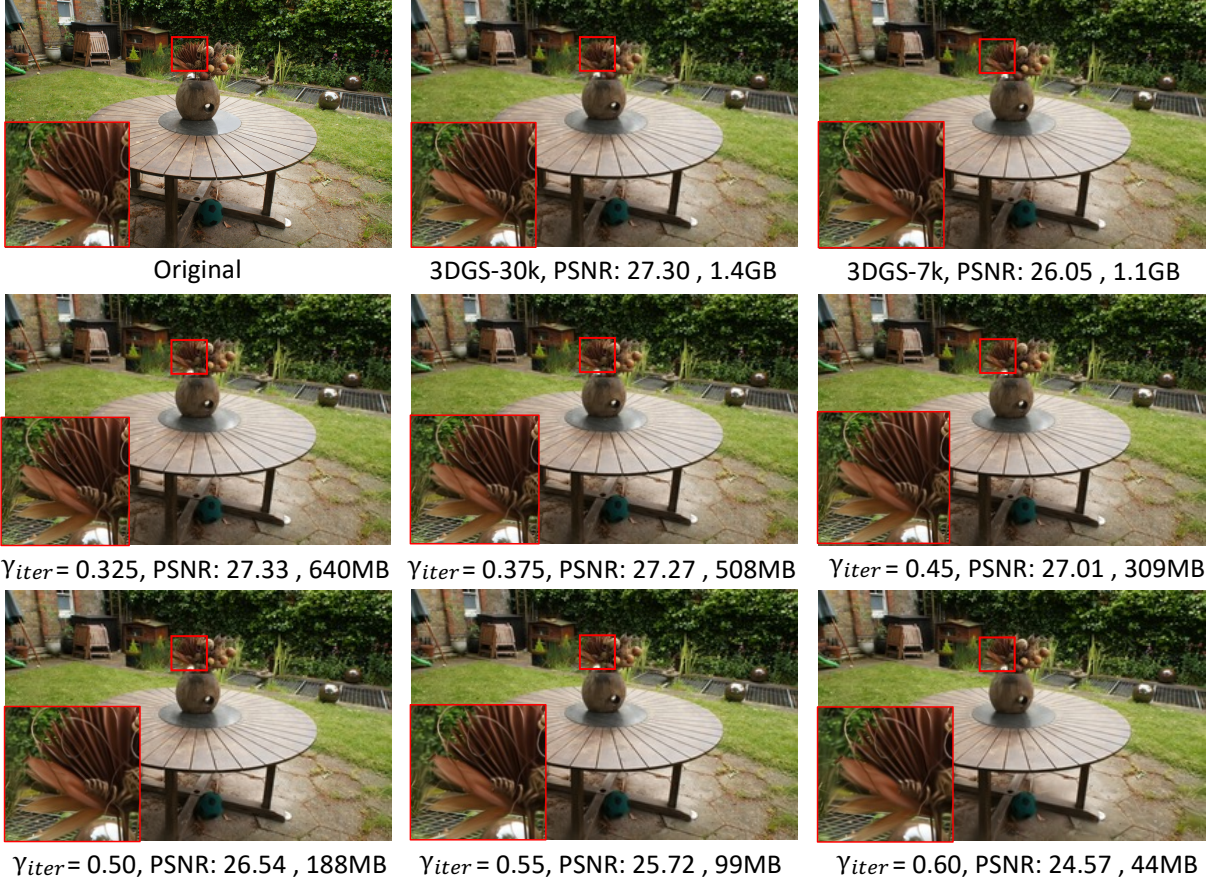


Figure 6: Qualitative comparison of the garden scene at various pruning levels ( $\gamma_{iter}$ ) using Trimming the Fat (gradient-aware iterative pruning). Our proposed method demonstrates substantially higher compression rates compared to both baselines while maintaining similar visual quality.

### 4.3 Ablation Study

**FPS Gain with Trimming the Fat.** Our novel pruning approach significantly enhances the FPS rate of 3DGS. On the Tanks&Temples dataset, our method achieves an FPS of over 600+ all while maintaining SOTA performance as shown in Fig. 7b. The renderings were performed using an RTX-3090, and the final FPS reported were averaged over three separate runs. These findings demonstrate the scalability of our proposed method.

**Why 3D Prior for Pruning is important?** To assess the significance of a 3D prior in the pruning process, we modified the original training protocol introduced by Kerbl *et al.* [10]. In their methodology, Gaussians are pruned and densified up to a specified iteration count (15k), employing an opacity threshold for pruning. Our modification involved halting the densification phase at the same iteration count (15k) but extending the pruning phase for an additional 10k iterations. Subsequently, the model underwent further fine-tuning for an additional 5k iterations to generate the final scene. The findings are outlined in Fig. 7a, indicating that even with a reduced pruning threshold, achieving convergence without a robust 3D prior remains challenging for a 3DGS model.

**Why Pruning is effective?** Our proposed pruning technique achieves compression ratios of up to 4 $\times$  without compromising performance compared to the 3DGS baseline. The efficacy of our approach lies in its ability to effectively eliminate redundant Gaussians. As depicted in Fig. 7c, the opacity distribution before and after pruning for the truck changes significantly. For the baseline 3DGS, the majority of opacity values are very low, indicating minimal contribution to scene reconstruction. However, through post-hoc pruning, a significant proportion of opacity values become notably higher, indicating that a more solid geometry is learned by the model.

**One Shot Pruning vs Iterative Pruning.** We also explored the impact of one-shot pruning in comparison to iterative pruning, in terms of model size, showcased in Fig. 7a. For one-shot pruning, we utilized the pre-trained 3DGS-30k model, performed the pruning process once, and then fine-tuned the model for 30k iterations.

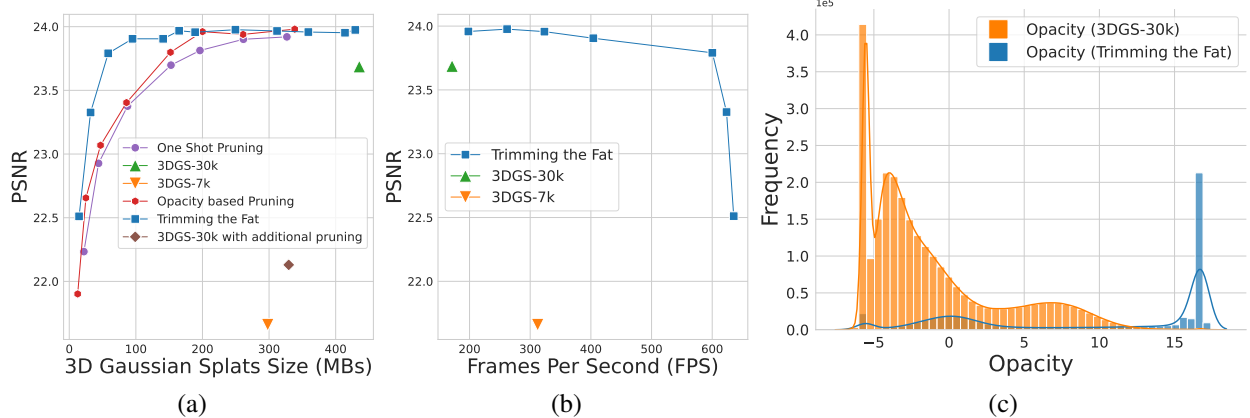


Figure 7: Trade-off between performance and size through iterative pruning and one-shot pruning techniques (a) and in terms of FPS on the Tanks&Temples dataset (b), and opacity distribution before and after pruning for the truck scene (c).

Table 2: Performance and compression comparison of 3DGS baseline, end-to-end compression [11], and our proposed method with the reference end-to-end compression method. Comp. stands for compression rate. <sup>†</sup> Reported from [11].

Mip-NeRF360					
Model	SSIM <sup>↑</sup>	PSNR <sup>↑</sup>	LPIPS <sup>↓</sup>	Mem <sup>↓</sup>	Comp. <sup>↑</sup>
3D Gaussian Splatting <sup>†</sup>	0.812	27.287	0.220	795.263	1×
End to End Compression [11] <sup>†</sup>	0.801	26.981	0.238	28.803	26.230×
Our's Trimming the Fat with End to End Compression	0.798	27.130	0.248	20.057	39.650×
Tanks&Temples					
Model	SSIM <sup>↑</sup>	PSNR <sup>↑</sup>	LPIPS <sup>↓</sup>	Mem <sup>↓</sup>	Comp. <sup>↑</sup>
3D Gaussian Splatting <sup>†</sup>	0.838	23.355	0.186	421.906	1×
End to End Compression [11] <sup>†</sup>	0.832	23.343	0.194	17.282	23.260×
Our's Trimming the Fat with End to End Compression	0.831	23.689	0.210	8.555	49.317×
Deep Blending					
Model	SSIM <sup>↑</sup>	PSNR <sup>↑</sup>	LPIPS <sup>↓</sup>	Mem <sup>↓</sup>	Comp. <sup>↑</sup>
3D Gaussian Splatting <sup>†</sup>	0.898	29.432	0.246	703.772	1×
End to End Compression [11] <sup>†</sup>	0.898	29.381	0.253	25.299	27.816×
Our's Trimming the Fat with End to End Compression	0.897	29.425	0.267	12.494	56.329×

Both gradient-aware and opacity-based iterative pruning consistently outperformed the one-shot pruning method: our results demonstrate that gradual pruning enables the model to better adapt to the scene compared to one-shot pruning.

**Trimming the Fat vs Compact3D [25].** Fig. 8 depicts a comparison of PSNR and Gaussian counts between our proposed approach and Compact 3D using the Tanks&Temples dataset. The results unequivocally highlight the superior performance of our method, demonstrating its capability to significantly reduce the number of Gaussians while maintaining baseline performance levels. These findings emphasize the effectiveness of our pruning technique and its potential to advance or replace existing compression methodologies for 3DGS.

**Lottery Ticket for the Gaussian Splats?** We investigated the potential presence of a “lottery ticket” phenomenon [32] for Gaussian splats. To test this hypothesis, we took an already pruned set of Gaussian splats from the Tanks&Temples dataset and randomly reinitialized all learnable features, including spherical harmonics (SH) features, opacity, scale, and rotation. Subsequently, we attempted to train these Gaussian splats for 30,000 iterations, but they failed to converge. This experiment underscores the necessity of having a learned 3D prior to which redundant

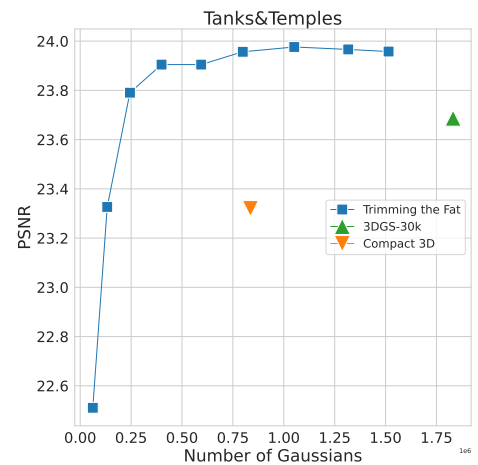


Figure 8: The graph illustrates the performance-size trade-off achieved by our method compared to the pruning approach proposed in Compact 3D [25] on the Tanks&Temples dataset.

dant information can be pruned. It highlights the difficulty of training Gaussian splats with the minimum number of Gaussians without any prior information from the 3D scene.

## 5 Conclusion

In this work, we presented a gradient-aware iterative pruning technique for 3D Gaussian splats named after ‘‘Trimming the fat’’. Our method effectively scales down Gaussian splats by a factor  $4\times$  without sacrificing generative quality. Particularly at higher pruning levels, our proposed method achieves compression ratios of approximately  $25\times$  and achieves up to 600 FPS with minimal impact on generative performance across established benchmark datasets. The resulting highly compressed point clouds can be seamlessly transmitted over networks and utilized on resource-constrained devices, offering potential applications in mobile VR/AR and gaming. Future research directions include investigating the integration of quantization-aware training methods to further improve the compressibility of 3DGS.

## References

- [1] Ben Mildenhall, Pratul P Srinivasan, Matthew Tancik, Jonathan T Barron, Ravi Ramamoorthi, and Ren Ng. Nerf: Representing scenes as neural radiance fields for view synthesis. *Communications of the ACM*, 2021.
- [2] Yi-Hua Huang, Yue He, Yu-Jie Yuan, Yu-Kun Lai, and Lin Gao. Stylizednerf: consistent 3d scene stylization as stylized nerf via 2d-3d mutual learning. In *Proceedings of the IEEE/CVF Conference on Computer Vision and Pattern Recognition*, 2022.
- [3] Chenxi Lola Deng and Enzo Tartaglione. Compressing explicit voxel grid representations: fast nerfs become also small. In *Proceedings of the IEEE/CVF Winter Conference on Applications of Computer Vision*, 2023.
- [4] Alex Yu, Vickie Ye, Matthew Tancik, and Angjoo Kanazawa. pixelnerf: Neural radiance fields from one or few images. In *Proceedings of the IEEE/CVF Conference on Computer Vision and Pattern Recognition*, 2021.
- [5] Berk Kaya, Suryansh Kumar, Francesco Sarno, Vittorio Ferrari, and Luc Van Gool. Neural radiance fields approach to deep multi-view photometric stereo. In *Proceedings of the IEEE/CVF Winter Conference on Applications of Computer Vision*, 2022.
- [6] Cheng Sun, Min Sun, and Hwann-Tzong Chen. Direct voxel grid optimization: Super-fast convergence for radiance fields reconstruction. In *Proceedings of the IEEE/CVF Conference on Computer Vision and Pattern Recognition*, pages 5459–5469, 2022.
- [7] Qiangeng Xu, Zexiang Xu, Julien Philip, Sai Bi, Zhixin Shu, Kalyan Sunkavalli, and Ulrich Neumann. Point-nerf: Point-based neural radiance fields. In *Proceedings of the IEEE/CVF conference on computer vision and pattern recognition*, 2022.
- [8] Thomas Müller, Alex Evans, Christoph Schied, and Alexander Keller. Instant neural graphics primitives with a multiresolution hash encoding. *ACM Transactions on Graphics (TOG)*, 41(4):1–15, 2022.
- [9] Sara Fridovich-Keil, Alex Yu, Matthew Tancik, Qinhong Chen, Benjamin Recht, and Angjoo Kanazawa. Plenoxels: Radiance fields without neural networks. In *Proceedings of the IEEE/CVF Conference on Computer Vision and Pattern Recognition*, 2022.
- [10] Bernhard Kerbl, Georgios Kopanas, Thomas Leimkühler, and George Drettakis. 3d gaussian splatting for real-time radiance field rendering. *ACM Transactions on Graphics*, 42(4), 2023.
- [11] Simon Niedermayr, Josef Stumpfegger, and Rüdiger Westermann. Compressed 3d gaussian splatting for accelerated novel view synthesis. *arXiv preprint arXiv:2401.02436*, 2023.
- [12] John Flynn, Ivan Neulander, James Philbin, and Noah Snavely. Deepstereo: Learning to predict new views from the world’s imagery. In *Proceedings of the IEEE Conference on Computer Vision and Pattern Recognition*, 2016.
- [13] Peter Hedman, Julien Philip, True Price, Jan-Michael Frahm, George Drettakis, and Gabriel Brostow. Deep blending for free-viewpoint image-based rendering. *ACM Transactions on Graphics (ToG)*, 37(6):1–15, 2018.
- [14] Gernot Riegler and Vladlen Koltun. Free view synthesis. In *Computer Vision–ECCV 2020: 16th European Conference, Glasgow, UK, August 23–28, 2020, Proceedings, Part XIX 16*. Springer, 2020.
- [15] Justus Thies, Michael Zollhöfer, and Matthias Nießner. Deferred neural rendering: Image synthesis using neural textures. *ACM Transactions on Graphics (TOG)*, 38(4):1–12, 2019.
- [16] Eric Penner and Li Zhang. Soft 3d reconstruction for view synthesis. *ACM Transactions on Graphics (TOG)*, 36(6):1–11, 2017.

[17] Philipp Henzler, Niloy J Mitra, and Tobias Ritschel. Escaping plato’s cave: 3d shape from adversarial rendering. In *Proceedings of the IEEE/CVF International Conference on Computer Vision*, 2019.

[18] Vincent Sitzmann, Justus Thies, Felix Heide, Matthias Nießner, Gordon Wetzstein, and Michael Zollhofer. Deepvoxels: Learning persistent 3d feature embeddings. In *Proceedings of the IEEE/CVF Conference on Computer Vision and Pattern Recognition*, 2019.

[19] Jonathan T Barron, Ben Mildenhall, Dor Verbin, Pratul P Srinivasan, and Peter Hedman. Mip-nerf 360: Unbounded anti-aliased neural radiance fields. In *Proceedings of the IEEE/CVF Conference on Computer Vision and Pattern Recognition*, 2022.

[20] Zhiqin Chen, Thomas Funkhouser, Peter Hedman, and Andrea Tagliasacchi. Mobilenerf: Exploiting the polygon rasterization pipeline for efficient neural field rendering on mobile architectures. In *Proceedings of the IEEE/CVF Conference on Computer Vision and Pattern Recognition*, 2023.

[21] Stephan J Garbin, Marek Kowalski, Matthew Johnson, Jamie Shotton, and Julien Valentin. Fastnerf: High-fidelity neural rendering at 200fps. In *Proceedings of the IEEE/CVF International Conference on Computer Vision*, 2021.

[22] Yihang Chen, Qianyi Wu, Jianfei Cai, Mehrtash Harandi, and Weiyao Lin. Hac: Hash-grid assisted context for 3d gaussian splatting compression. *arXiv preprint arXiv:2403.14530*, 2024.

[23] Ben Fei, Jingyi Xu, Rui Zhang, Qingyuan Zhou, Weidong Yang, and Ying He. 3d gaussian as a new vision era: A survey. *arXiv preprint arXiv:2402.07181*, 2024.

[24] Tao Lu, Mulin Yu, Lining Xu, Yuanbo Xiangli, Limin Wang, Dahua Lin, and Bo Dai. Scaffold-gs: Structured 3d gaussians for view-adaptive rendering. *arXiv preprint arXiv:2312.00109*, 2023.

[25] Joo Chan Lee, Daniel Rho, Xiangyu Sun, Jong Hwan Ko, and Eunbyung Park. Compact 3d gaussian representation for radiance field. *arXiv preprint arXiv:2311.13681*, 2023.

[26] Matthias Zwicker, Hanspeter Pfister, Jeroen Van Baar, and Markus Gross. Ewa volume splatting. In *Proceedings Visualization, 2001. VIS’01*. IEEE, 2001.

[27] Shimon Ullman. The interpretation of structure from motion. *Proceedings of the Royal Society of London. Series B. Biological Sciences*, 203(1153), 1979.

[28] Sara Fridovich-Keil, Giacomo Meanti, Frederik Rahbæk Warburg, Benjamin Recht, and Angjoo Kanazawa. K-planes: Explicit radiance fields in space, time, and appearance. In *Proceedings of the IEEE/CVF Conference on Computer Vision and Pattern Recognition*, 2023.

[29] Davis Blalock, Jose Javier Gonzalez Ortiz, Jonathan Frankle, and John Guttag. What is the state of neural network pruning? *Proceedings of Machine Learning and Systems*, 2020.

[30] Blake Woodworth, Suriya Gunasekar, Jason D Lee, Edward Moroshko, Pedro Savarese, Itay Golan, Daniel Soudry, and Nathan Srebro. Kernel and rich regimes in overparametrized models. In *Conference on Learning Theory*. PMLR, 2020.

[31] Arno Knapitsch, Jaesik Park, Qian-Yi Zhou, and Vladlen Koltun. Tanks and temples: Benchmarking large-scale scene reconstruction. *ACM Transactions on Graphics (ToG)*, 36(4):1–13, 2017.

[32] Jonathan Frankle and Michael Carbin. The lottery ticket hypothesis: Finding sparse, trainable neural networks. In *7th International Conference on Learning Representations, ICLR 2019, New Orleans, LA, USA, May 6-9, 2019*.